

1 Identification of the cloud base height over the Himalayan 2 mountain range: Intercomparison of Ceilometer and Doppler 3 Lidar

4
5
6 K.K. Shukla^{1,2}, K. Niranjana Kumar³, D.V. Phanikumar¹, Rob K Newsom⁴, V. R. Kotamarthi⁵
7 Taha B.M.J. Ouarda^{3,6} and M. Venkat Ratnam⁷
8

9 ¹Aryabhata Research Institute of observational sciences, Nainital, India

10 ²Pt. Ravishankar Shukla University, Raipur, Chhattisgarh, India

11 ³Institute Center for Water and Environment, Masdar Institute of Science and Technology, Abu Dhabi, United Arab
12 Emirates

13 ⁴Pacific Northwest National Laboratory, Richland, Washington, USA

14 ⁵Argonne National Laboratory, Argonne, Illinois, USA

15 ⁶INRS-ETE, Quebec City (Qc), Canada

16 ⁷National Atmospheric Research Laboratory, Gadanki, Tirupati, India

17 *Correspondence to:* D V Phanikumar (phani@aries.res.in; astrophani@gmail.com)
18

19 **Abstract.** We present the measurement of cloud base height (CBH) derived from the Doppler Lidar (DL),
20 Ceilometer (CM) and Moderate Resolution Imaging Spectroradiometer (MODIS) satellite over a high altitude
21 station in the Himalayan **mountain range** region for the first time. We analyzed six cases of cloud overpass during
22 the daytime convection period by using the cloud images captured by **Total Sky Imager (TSI)**. The occurrence of
23 thick clouds (> 50%) over the site is more frequent than thin clouds (< 40 %). In every case, the CBH **is located** less
24 than 1.2 km, above ground level (AGL) observed by both DL and CM instruments. The presence of low level clouds
25 in the height-time variation of signal to noise ratio of DL and backscatter of CM shows a similar pattern on all days.
26 Cloud fraction is found to be maximum during the convective period. The CBH estimated by the DL and CM
27 showed reasonably good correlation ($R^2=0.81$). The DL observed updraft fraction and cloud base vertical velocity
28 also shows good correlation ($R^2=0.71$). The inter-comparison between DL and CM will have implications in filling
29 the gap of CBH measurements by the DL, in absence of CM. More deployments of such instruments will be
30 invaluable for the validations of meteorological models over the observationally sparse Indian regions.
31

32 **Key words:** Cloud base height, Doppler Lidar, Ceilometer, Radiosonde
33
34
35

1 **1. Introduction**

2 The Earth's shortwave and longwave radiation at the surface and as well as the top of the atmosphere is influenced
3 by cloud macrophysical properties such as cloud coverage and cloud base height (CBH) (Considine et al., 1997;
4 Meerkötter and Bugliaro, 2009). The formation of all-weather clouds occurs in lowest layer of the atmosphere (i.e.
5 troposphere). The extensive occurrence of stratocumulus and stratus clouds over ocean (~34%) and land surface
6 (~18%) in the lower atmosphere and near the atmospheric boundary layer (ABL) is well documented (Heymsfield,
7 1993; Considine et al., 1997). It was found that there is an increase in planetary albedo and a decrease in shortwave
8 radiation at the surface due to ABL clouds (Heymsfield, 1993; Berg and Kassianov, 2007). Moreover, clouds can
9 also affect the structure of atmospheric parameters like ABL height, temperature and relative humidity because of
10 their vital role in altering the water cycle over the Earth's surface and play a critical role in the removal of
11 atmospheric pollutants through precipitation (Ghate et al., 2011).

12 A strong coupling is observed between the ABL cumulus clouds and associated turbulence in the ABL,
13 which have impact on the ABL diurnal variability (Stull, 1985; Brown et al., 2002). These clouds can be lifted more
14 than a few hundred meters due to the ABL evolution during morning to the afternoon hours over the land
15 (Meerkötter and Bugliaro, 2009). **During daytime, more updrafts are dominant. This has been reported in the**
16 **past by various researchers by using the Doppler Lidar (DL) vertical velocity observations (O'Connor et al.,**
17 **2010; Harvey et al., 2013; Schween et al., 2014). Schween et al., 2014 studied the mixing layer height (MLH)**
18 **by using DL vertical velocity standard deviation and Ceilometer (CM) aerosols backscatter as this layer plays**
19 **an important role in the atmospheric dynamics. They have proven that CM is a potential instrument for the**
20 **estimation of MLH by using aerosols as proxy and also cloud base height (CBH).** The cloud top height can be
21 retrieved with different retrieval algorithms (Forsythe et al., 2000; Hutchison, 2002; Huang et al., 2006; Weisz et al.,
22 2007) for use with various satellite observations such as the Cloud-Aerosol Lidar and Infrared Pathfinder Satellite
23 Observations (CALIPSO) (Winker et al., 2003), CloudSat and Tropical Rainfall Measuring Mission (TRMM)
24 (Stephens et al., 2002; Kummerow et al., 1998).

25 Due to the various feedbacks between clouds, radiation and dynamics described above, it is extremely
26 important to have the simultaneous observations of the clouds and vertical velocity in the Earth's atmosphere for the
27 appropriate representation in the Global Circulation Models (GCMS) (Randall et al., 1985; Tonttila et al., 2011).
28 The vertical structure of convective and cumulonimbus clouds are studied by using precipitation radar over the south
29 Asian region (Bhat and Kumar, 2015). **An appropriate detection of CBH by using CM is very important for**
30 **various scientific applications. Different methodologies for the detection of CBH using different sensors have**
31 **been proposed by several researchers (e.g. by using gradient method on backscatter profile (Martucci et al.,**
32 **2010), threshold method (Van Tricht et al., 2014), multisensor, approaches as in Cloudnet (Illingworth et al.,**
33 **2007) and visibility based methods like Väisälä laser CM ((Väisälä Oyj (2002) and Morris (2012))). The**
34 **retrieval algorithms used for the CBH and their reliability by using CM depends on a number of factors (i.e.**
35 **used CBH detection algorithm (Martucci et al., 2010), type of cloud hydrometeors (Van Tricht et al., 2014),**
36 **sensor wavelength and likely its sensitivity (Schween et al., 2014)). This has been investigated by several**

1 **researchers in the past.** Sharma et al., (2016) studied the CBH observed by using CM during 2013-2015 over the
2 western site in India and also compared with the Moderate Resolution Imaging Spectroradiometer (MODIS)
3 satellite. The observed CBH by ground-based (CM) and space-based satellite (MODIS) observations showed good
4 correlation over the western Indian site.

5 **As Manora Peak (29.4° N; 79.2° E; 1958 m above mean sea level (amsl)), Nainital is located on the**
6 **mountain top. It is considered as a high altitude site in the Himalayan region and it also lies in the sub-tropic**
7 **region which is influenced by the Indian summer monsoon. The local orography of the site itself plays an**
8 **important role in the formation of the clouds over the site. Therefore, it becomes an important site to study**
9 **the factors affecting the Indian monsoon (i.e. aerosols and clouds etc.).** In addition, observations of vertical
10 velocity remain sparse over most of the site in the Indian region and in particular over regions with the high altitude
11 and complex topography. The **Atmospheric Radiation Measurements (ARM) Mobile Facility (AMF1)** conducted
12 a field campaign during June 2011-March 2012 over a high altitude site Manora Peak, Nainital to have a better
13 understanding about the cloud, precipitation and aerosols in the Ganges basin, i.e. Ganges Valley Aerosol
14 eXperiment (GVAX). During GVAX, different ground based remote sensing instruments were operated to measure
15 the atmospheric dynamical parameters. A DL was continuously operated to measure the vertical velocity and
16 backscatter from the ABL clouds. Along with the DL, CM and TSI were also operated continuously to measure
17 CBH and to capture the cloud images, respectively, in the daytime over the observational site.

18 In the current study, our main objective is to evaluate the capability of DL in estimating the CBH and
19 comparing the results with CM, the standard instrument for the CBH measurement and CBH derived from the
20 MODIS. The advantage of DL over the other two measurements is that one can get the simultaneous information on
21 both vertical velocities near clouds along with the CBH. In this study, we have considered six selected cases based
22 on cloud coverage, residence time of clouds and availability of simultaneous datasets with other ground based
23 instruments over the site during the observational period (05-10 UT).

24 **2. Observational site, instrumentation and methodology**

25

26 Ganges valley region of the Indian subcontinent is a heavily populated region and shows an increase in the
27 **pollutants level** in the current **scenario** (Ramanathan et al. 2005; Lau and Kim 2006; Bollasina et al., 2011).
28 Bollasina et al., (2011) showed the increment in the concentration of anthropogenic aerosols over the Ganges valley
29 region which has the ability to modify the Indian Summer Monsoon (ISM) rainfall. To understand **the change in**
30 **ISM** over the Indo-Gangetic Plain (IGP), the geographical location of Manora Peak (29.4° N; 79.2° E; 1958 m
31 amsl), Nainital is suitable for measuring the various atmospheric parameters in campaign mode. To have a better
32 understanding of the impact of measured parameters like aerosol, convection, cloud, and radiative characteristics of
33 the Indian monsoon, Atmospheric radiation measurement (ARM) mobile facility conducted a field campaign over
34 the site which is known as Ganges Valley Aerosol Experiment (GVAX) (Kotamarthi, 2010). The GVAX campaign
35 was utilized to quantify the impact of aerosols on ISM, role of atmospheric boundary layer in aerosol transportation
36 in the Ganges valley region and also the effect of aerosols in the cloud formation. By considering all the above

1 serious issues, the current observational site is selected to conduct the campaign mode observations (Kotamarthi,
2 2013).

3 **Manora Peak, Nainital** is away from the urban/industrial pollution. The total population of the Nainital is ~ 0.5
4 million (according to census 2011) with population density ~ 50 persons per km². The small-industries having cities
5 i.e. Haldwani and Rudrapur are located ~20-40 km away in the south of the observational site. A mega city, New
6 Delhi, the capital of India is located ~ 225 km in the southwest of the study region (Sagar et al., 2015). The site is
7 surrounded by a dense forest. The maximum and minimum temperatures are observed to be ~ 1 °C and 20 °C during
8 winter (December January February) and pre-monsoon (March April May) seasons, respectively (Sarangi et al.,
9 2014; Dumka et al., 2014; Shukla et al., 2014). Singh et al., 2016 observed the maximum/minimum rainfall
10 during of July (367.0 mm)/September (222.3 mm) in the summer monsoon season over the site respectively. It
11 is also observed that the 9% of total rainfall during summer monsoon (1440 ± 430 mm) period is observed in
12 the rest months (October 2011-March 2012) of the GVAX over the site. It is also observed that the low level
13 clouds during the Indian summer monsoon (surface-2 km, AGL, ~70%) play major role in the total rainfall
14 over the observational site. The single layer clouds are more dominant during the GVAX period over the site
15 (Singh et al., 2016). Moreover, wind patterns over the site during monsoon and winter are southwesterly and
16 northwesterly, respectively. The seasonal change in wind pattern every year persists over the Indian subcontinent
17 (Asnani, 2005). The detailed description about the site and current research works carried out over the observational
18 site can be found in detail in Sagar et al. (2015) and Singh et al., 2016.

19 **Although, the ARM deployment over the site was carried out during June 2011-March 2012, we do**
20 **not have the DL data during the monsoon (June-September 2011) period because of washout of the aerosol**
21 **particles over the Manora Peak, Nainital. Moreover, we have both no/less percentage of cloud coverage and**
22 **less cloud residence time (~1-2 hours) during other seasons. Hence, we have particularly selected those cases**
23 **where cloud coverage and residence times are maximum during the daytime (05-10 UT) which is mostly the**
24 **convection dominant period. It is also to be noted the complexity in deriving CBH with the DL which is first**
25 **of its kind over the Himalayan region. Also, another aspect for selecting these cases is the availability of**
26 **simultaneous datasets with other instruments like CM, Radiosonde and other meteorological instruments.**
27 **Some of the cases are rejected because of sudden spikes and other consistency checks.**

28 2.1 Total Sky Imager (TSI)

29 The TSI is manufactured by Yankee Environmental Systems (YES), and is commercialized version of the
30 **Hemispheric Sky Imager** prototype (Long et al., 2006). The TSI-660 was deployed by **AMF1** over the Manora
31 Peak, Nainital during the GVAX to capture the cloud images during the daytime. The sky cloud images captured by
32 TSI are 24-bit color JPEG images at 650x480 pixel resolution. TSI captures the cloud image at every 30 sec during
33 daytime. In order to retrieve cloud information, we have **used the** processed raw cloud images **and also retrieved**
34 **cloud parameters by the manufacture** of the TSI. Sky cover retrieval from TSI images is valid only for solar
35 elevation angles >3⁰ (zenith angles < 80⁰) and images are processed for a 160⁰ field of view, ignoring the 10⁰ of sky

1 near the horizon. It has a sun-blocking strip mask, which represents the location of the sun with a yellow dot in the
2 image. We have used TSI images to infer the presence of clouds over the site for a subsequent CBH estimate. The
3 TSI observations of cloud images are also utilized for the estimation of percentage of thin and opaque clouds over
4 the site. **The scattering of blue light is more than red in clear skies and no aerosols conditions (i.e. molecular
5 scattering). The red pixel values of the TSI images are much higher in the presence of clouds over the imager
6 in comparison to no cloud conditions. Clear/Thin determines the ratio of thin cloud cover to clear sky.
7 Thin/Opaque determines the ratio of thin cloud cover to opaque cloud cover. The values are assigned upon
8 initial configuration of the TSI by adjusting each ratio to match the cloud in observed images. We prefer to
9 assign these values during mixed-phase clouds near solar noon. We have used the data in the current study
10 which is retrieved by the manufacture by using standard methods for the TSI. Detailed discussion about the
11 estimation of cloud properties by using TSI images were given in previous reports (Long et al., 2001, 2006;
12 Morris, 2005).**

13 **2.2 Doppler Lidar**

14
15 DL was operated over a high altitude site **Manora Peak, Nainital** to measure the temporal and altitude resolved
16 vertical velocity and attenuated backscatter. **Detailed descriptions of the technical characteristics of the DL are
17 given in Table-1.** In order to retrieve the radial velocity by using Doppler principle, DL uses aerosols as tracer in
18 the atmosphere to observe the Doppler shift. The influence of insects or pollen is less in the DL observations
19 because the small aerosols in the background dominate the signal. The DL uses an eye-safe laser of wavelength ~ 1.5
20 μm . It provides the vertical velocity and attenuated backscatter at a spatial resolution of $\sim 30\text{m}$ and a temporal
21 resolution of 1 sec. The DL can scan the atmosphere in different modes (i.e. vertically Fixed-Beam Stare (FPT),
22 Range-Height Indicator (RHI) scan and Plan-Position Indicator (PPI) scan mode). The RHI and PPI scan modes are
23 known as the elevational and azimuthal scan of the atmosphere, respectively. A detailed technical description of the
24 DL system can be found in previous studies (Pearson et al., 2009; Newsom, 2012; Shukla et al., 2014). In the current
25 study, the vertically fixed-beam stare mode of the DL is used to estimate CBH. **To minimize/remove random noise
26 fluctuations in the DL data, a threshold on the signal to noise ratio (SNR) of -20 dB is applied. In order to find
27 an appropriate SNR threshold for DL dataset, we have followed the methodology described in detail in
28 Lenschow et al., (2000) and Pearson et al., (2009). Additional data error analysis explanation can be found in
29 Newsom et al., 2015. The reduction in the SNR threshold values also lead to an increase of 50% in the data
30 accessibility (Manninen et al. 2016).**

31

32 **2.3 Laser Ceilometer**

33

34 The Väisälä laser Ceilometer (CT25K) is deployed over the site for precise measurements of the CBH, vertical
35 visibility and vertical profile of aerosol backscatter during GVAX (Väisälä Oyj, 2002). It has an eye-safe laser
36 source of wavelength $\sim 905\text{ nm}$. It provides the information at a temporal resolution of 16 sec and a spatial resolution

1 of 30 m in the atmosphere (Morris, 2012). The 16 sec interval data is aggregated to 1 min for better comparison with
2 the DL. **The detailed description of the technical properties of the CT25K Ceilometer which was used by**
3 **various investigators in the past is available in M \ddot{u} nk \ddot{u} l et al., 2007, 2011; Haeffelin et al., 2012; Schween et al.,**
4 **2014 and Wiegner et al., 2014. Weigner et al., (2014) showed that the observed aerosol backscatter by using**
5 **CM have significant error due to various sources i.e. 10% due to change in calibration constant of the CM, ~**
6 **20 % due to water vapor distribution in the atmosphere.**

8 **2.4 Surface Meteorology System**

9
10 The in-situ sensors are used to measure the surface temperature (T), relative humidity (RH), pressure, wind speed
11 and wind direction by the ARM surface meteorology systems (MET). The in-situ sensors are installed at specific
12 standard heights for measurement of meteorological parameters (i.e. T & RH at 2 m; Barometric pressure at 1 m and
13 wind speed and direction at 10 m) (Ritsche and Prell, 2011). The MET sensors provide the data at a temporal
14 resolution of 1-min and we have averaged for 10-min from 1-min data to calculate the lifted condensation level
15 (LCL) for comparison with the CBH of DL and CM, respectively.

17 **2.5 Radiosonde**

18
19 V \ddot{a} is \ddot{a} l \ddot{a} Radiosondes (RS-92) were launched during GVAX at 00, 06, 12 and 18 UT daily regularly. The profiles of
20 atmospheric parameters (temperature, relative humidity and winds) are measured by the Radiosonde (RS) at a
21 vertical resolution of 10 m as the ascent rate of balloon is 5 ms⁻¹ and transmitter time resolution is 2 sec. In the
22 current study, we have used the 06 UT (11.5 hr LT) data of RS to calculate the LCL for all the cloud cases. The
23 detailed description about the RS can be found in previous reports (Holdridge et al., 2011; Shukla et al., 2014).

25 **2.6 Moderate Resolution Imaging Spectroradiometer**

26
27 In addition to the ground based remote sensing techniques used for the estimation of CBH, we have also utilized the
28 MODIS satellite derived CBH over the observational site. The MODIS Terra data is obtained for the same cases as
29 measured by the ground based remote sensing instruments. **We have used the MODIS level 3 (MOD08_D3.051)**
30 **data in the current study.** However, the spatial resolution of MODIS cloud data is of 1^o x 1^o latitude-longitude
31 grids. We have used the cloud top pressure, cloud optical depth and effective radius of liquid cloud for all the cases.
32 **A detail description of the MODIS data is given for instance in Kishcha et al., (2007) and Platnick et al.,**
33 **(2015).**

35 **3. Retrieval of Cloud base height (CBH) and Lifting Condensation Level (LCL)**

37 **3.1 Cloud Statistics from the DL**

1 We have used the vertical velocity and cloud statistics derived data of the DL during GVAX (Newsom et al., 2015).
2 In addition to clear-air vertical velocity statistics, we can derive the CBH, cloud fraction, cloud base vertical velocity
3 and cloud base updraft fraction. For the current **dataset, the vertical velocity and cloud statistics value added**
4 **product (VAP) uses a 30-minute averaging time window, but produces output using a 10-minute sampling**
5 **interval. Thus, every third sample is statistically independent. The** cloud fraction is the fraction of time during
6 the averaging interval that a cloud is detected at any height. Similarly, the cloud base updraft fraction is the fraction
7 of time that a positive (upward) cloud base vertical velocity is observed during the averaging interval. **CBH**
8 **estimates are obtained by locating the heights of sharp spikes in the 1-sec range-corrected SNR profiles, as**
9 **illustrated in Figure 4. To minimize false detections, the CBH algorithm uses a method based on the first**
10 **derivative of the range-corrected SNR. When a cloud is present in the profile, the first derivative, which is**
11 **computed using a simple central-difference approximation, shows a strong positive peak immediately below**
12 **and a strong negative peak immediately above the cloud base. We require the magnitude of these peaks to**
13 **exceed 0.1 km, and separation to be between 2 and 15 range bins. If these conditions are satisfied, then the**
14 **algorithm locates the maximum in the range-corrected SNR between these two extrema. The height of this**
15 **maximum then determines the CBH. This process is then repeated for all 1-sec profiles acquired during a**
16 **given 24-hour period. Additional checks are then applied to minimize false detections by rejecting temporally**
17 **isolated CBH estimates. This is done by computing the absolute difference in CBH between a given profile**
18 **and the CBH values from profiles located immediately before and after in time. If both differences exceed**
19 **1km then that CBH value is rejected. Once the CBH values have been determined in this way, the cloud base**
20 **vertical velocity is determined from the vertical velocity at the CBH. The vertical velocity and cloud statistics**
21 **VAP reports the median value of the 1-sec CBH values and cloud base vertical velocities over a given 30-min**
22 **averaging interval. Further details are given in Newsom et al. (2015).**

23

24 **3.2 CBH retrieval by using CM**

25

26 The measurement of the CBH with CM is known as standard method of the ground-based active remote sensing
27 technique. The time delay between the transmitted and backscattered signal from the haze, fog, virga, mist and
28 precipitation to the receiver of CM can be used to estimate the CBH. By knowing the time delay in equation (1),
29 CBH can be estimated as **function of height with atmospheric visibility threshold**

30

$$\text{Cloud base height (h)} = (c*t/2) \quad (1)$$

31

32 where $c (= 3 \times 10^8 \text{ m s}^{-1})$ is the speed of light and t is the time delay. The backscattering coefficient is estimated by
33 using the strength and attenuation of the backscattered signal from the atmosphere. Cloud base is identified by the
34 strong increase of the backscatter coefficient and three layers of clouds can be detected if the lower clouds are
35 transparent (Emeis et al., 2009; Morris, 2012). **Flynn, (2004) have developed an algorithm to determine the**
36 **cloud base as the height when they have observed a reduction in the visibility order of 100 m in the**
37 **atmosphere. We have used the standard output of CBH from Väisälä laser Ceilometer (CT25K) and it uses**

1 the visibility threshold method for CBH (Väisälä Oyj, 2002). The CeiLinEx (Ceilometer Performance
 2 Experiment at Lindberg: <http://ceilinex2015.de/special-topics/test>.) 2015 showed that the retrieval of CBH
 3 leads to different results with the different algorithms.

4 3.3 CBH Retrieval by MODIS

5
 6 The estimation method of the CBH by using MODIS is described in detail by Hutchison (2002) and Sharma et
 7 al., (2016). In order to estimate the CBH over the Manora Peak by using the MODIS Terra dataset, we have
 8 used the cloud top pressure, cloud optical thickness, effective radius of the water cloud particle and liquid
 9 water path during daytime from MODIS Terra satellite over the observational site for cloud passages
 10 observed by the TSI. The CBH from the MODIS is calculated by taking the difference between the cloud top
 11 height and the thickness of cloud (ΔZ) which is given in equation (2).

$$12 \quad Z_{\text{Cloud base height}} = Z_{\text{Cloud top height}} - (\Delta Z) \quad (2)$$

13 where ΔZ is the cloud thickness and ΔZ is ratio of LWP and LWC.

14 The thickness of water cloud depends on the relation between liquid water path (LWP) and liquid water
 15 content (LWC). Liou (1992) showed that the relation of cloud optical thickness (τ) and effective radius of cloud
 16 particle size (r_{eff}) with LWP is given by

$$17 \quad \text{LWP} = (2 * \tau * r_{\text{eff}}) / 3 \text{ g.m}^{-2} \quad (3)$$

18 LWC=0.26 g.m⁻³ taken for cumulus cloud in clean condition (Hess et al., 1998).

$$19 \quad \Delta Z = (\text{LWP} / \text{LWC}) \quad (4)$$

20 By using LWP & LWC in equation (4), we have calculated the thickness of cloud (ΔZ).

21 We have estimated the CBH for water cloud present in the atmosphere by using equation (2) & (4).

23 3.4 Lifted condensation level estimation by using surface MET and RS datasets

24
 25 The estimation of water vapor content from surface MET data has been derived by using equation (5) with T and
 26 RH of surface meteorology (Goff-Gratch, 1946).

$$27 \quad e_s = e_{st} * 10^Z \quad (5)$$

28 where

$$29 \quad Z = A \left(\frac{T_s}{T} - 1 \right) + B \times \log_{10} \left(\frac{T_s}{T} \right) - C \times \left[10^{D \left(1 - \frac{T}{T_s} \right)} - 1 \right] + F \left[10^{H \left(\frac{T_s}{T} - 1 \right)} - 1 \right]$$

30
 31 and A = -7.90298, B= 5.02808, C=-1.3816 X 10⁻⁷, D= 11.344, F=8.1328 X 10⁻³, H= -3.49149 are the constants. e_{st}
 32 (=1013.246 mb) is saturation vapor pressure (e_s) at boiling temperature ($T_s=373.16$ K) at standard atmospheric
 33 pressure. By using saturation vapor pressure (e_s) from equation (5) and surface RH in equation (6), we have
 34 calculated the water vapor pressure (e)

1
$$RH = \left(\frac{e}{e_s} \right) \times 100 \quad (6)$$

2 Dew point temperature (T_d) estimation by using surface MET vapor pressure (e) is given by the equation (7) **and it**
 3 **is taken from the Lawrence, (2005)**

4
$$T_d = \left(\frac{1}{\left[\left(\frac{1}{T_0} \right) - \left(\frac{R_v}{L} \right) \ln \left(\frac{e}{e_0} \right) \right]} \right) \quad (7)$$

5 where $T_0=273$ K, $e_0 = 0.611$ kPa, $\frac{R_v}{L} = 0.0001844$ K⁻¹, e - vapor pressure

6 By knowing the temperature (T) and dew point temperature (T_d) from surface meteorology and RS, we have
 7 calculated LCL by using equation (8)

8
$$\text{Lifting Condensation level (LCL) height (km)} = 0.125 * (T - T_d) \quad (8)$$

9
 10 **The well-mixed ABL air parcels which have a dry-adiabatic temperature profile and a constant mixing ratio**
 11 **are used to determine the LCL profile (Craven et al., 2002). For the detection of CBH, the LCL is a good**
 12 **approximation as the CBH depends on the relative humidity and temperature near the surface. The LCL**
 13 **depends on the temperature and dew point temperature above the surface and is thus a good proxy for CBH.**

14
 15 **4. Results and discussion**

16
 17 Figure 1 shows one of the six (12 October 2011, 21 November 2011, 11 December 2011, 20 January 2012, 08
 18 February 2012 and 14 March 2012) cloud case examples considered in this study observed by TSI for the estimation
 19 and comparison of CBH by different instruments over the observational site. It shows the raw (Figure 1a) and
 20 masked (Figure 1b) cloud images by TSI at hourly interval during daytime from (10.5-15.5 hr) on 12 October 2011.
 21 The “yellow dot” in the TSI masked image represents the position of the sun, not obscured by the clouds. However,
 22 if this “yellow dot” becomes “white” then the sun is obscured completely by the clouds (Figure 1b; Pfister et al.,
 23 2003). **There is a difference between the raw and masked images. In masked images, TSI software masks out**
 24 **obstructions-the imager, its arm and the sun-blocking band in the raw images.** It is also to be noted that the
 25 presence of cloud is clearly apparent with the raw image of the sky captured by TSI (Figure 1a). However, the
 26 masked images strongly confirm the presence of clouds and further distinguish between the thin and opaque clouds
 27 by the color of the image. For instance, the blue, gray, and white colors in Figure 1b represent the cloud free-sky,
 28 thin and opaque clouds, respectively. While the black color in Figure 1b represent the masked pixels which are not
 29 used in determining the macrophysical property of cloud by the TSI. Temporal variation of masked images of clouds
 30 captured by TSI for all cases in the 160° field of view (FOV) centered at zenith in the cloud images during 10.5-15.5
 31 LT is shown in Figure 2. Due to masked sky images, the loss of about 17 % of the hemispherical solid angle of the
 32 sky dome is resulted. In the analysis of clear/cloudy pixels, these masked ‘black’ parts are ignored (Long et al.,
 33 2006). From Figure 2, it is clearly seen that there are lesser clouds in the forenoon (before 12.5 LT) in comparison

1 to afternoon (after 12.5 LT) on 12 October, 21 November and 11 December 2011. We have observed the clouds at
2 every hour on 20 January, 08 February and 14 March 2012. In Figure 3 (a-f), we also show the temporal variation of
3 the percentage occurrence of thin (shown by black line with black open circle) and opaque clouds (red line with red
4 open rectangle) for all the six cloud overpasses over the observational site. In most of the cases of figure 3(a-f), the
5 percentage of opaque clouds are greater than percentage of thin clouds. **The dominance of opaque and thin clouds**
6 **is clearly seen from the figure 3(a-f) during daytime over the site.** It is also evident from Figure 3 that the
7 percentage occurrence of opaque clouds is more frequent over the site relative to the thin clouds during the
8 observational period.

9 Figures 5 (a1-f1) and (a2-f2), illustrate the height-time variation of SNR and backscatter for different cases
10 of cloud passage over the observational site observed by DL and CM, respectively. Figure 5 depicts the presence of
11 ABL clouds over the site. The development of convective clouds in the lowest part of ABL is due to the presence of
12 convective thermals. These convective thermals are crucial in the formation of the clouds because these thermals can
13 rise from the surface to the top of the mixing layer without being diluted (Crum and Stull, 1987). It should be noted
14 that the presence of the convective clouds in the ABL can be confirmed by using the observed CBH from DL and
15 CM and lifted condensation level (LCL) estimated from the surface (Stull and Eloranta, 1985; Zhang and Klein,
16 2013). During the convection, the maximum SNR is observed due to the presence of low level ABL cumulus clouds.
17 Also, the observed cloud cases show different dynamics of the cumulus clouds over the site. Figure 5(a1) shows the
18 SNR maximum around 11.5-12.5 LT showing high percentage of opaque cloud during 12.5-14.5 LT and then
19 dominated by a thin clouds, consistent with Figures 5(a1) and 5(b1). Other cases also depict similar variation with
20 opaque clouds more frequent than the thin clouds during convection (see Figures 5b1-f1). Similarly, Figure 5 (a2-f2)
21 shows the height-time variation of averaged backscatter ($\text{srad}^{-1} \cdot \text{km}^{-1} \cdot 10^{-4}$) by the CM observed for all cloud cases in
22 the study. It is interesting to note that the temporal evolution and duration of thin and opaque clouds **observed by**
23 **the TSI** are in reasonable agreement **with the DL and CM cloud pattern** during all events.

24 In Figure 6 (a-f), we have plotted the temporal variation of CBH (with DL & CM) and cloud occurrence
25 frequency (with DL). The detailed description about the estimation of CBH is given in the section 3.1. The
26 fraction of time that a cloud is detected at any altitude during the given averaging period is defined as cloud
27 frequency. Varikoden et al. (2011) showed that the occurrence of low level clouds are more in comparison to the
28 mid-level clouds by using CM over a tropical station Akkulam, Thiruvananthapuram (8.29° N, 76.59° E, 15 m
29 above sea level) in India. They have also showed that the occurrence of low level clouds is higher during the
30 afternoon hours. We have also found that the frequency of occurrence of clouds are showing different
31 characteristics during forenoon and afternoon in the observed cases with both CM and DL over a high altitude
32 site.

33 Figure 7 (a-f) depicts the temporal variation of CBH observed by the DL and CM along with lifted
34 condensation level (LCL) height estimated by using surface MET parameter and RS **for all the selected case**
35 **examples in the current study.** There is a strong co-relation between the CBH observed by the DL and CM for all
36 cases. On an average, the CBH from both the instruments is higher during the convective period and is associated
37 with the change in LCL in the ABL during daytime. We have estimated the LCL with surface MET and RS to

1 compare with the CBH of DL and CM. In 12 October 2011 case, a small difference is observed between the CBH
2 (DL) and LCL heights but LCL heights with the MET and RS shows a similar pattern as CBH (CM) implying the
3 strong association with ABL dynamics (Jones et al., 2011). From Figure 7 (a-f), it is clearly observed that in all the
4 cases, CBH is coupled with the LCL estimated from the surface meteorological parameters. This strong dependence
5 of CBH with LCL suggests the link between cloud formation and development of convection on the surface (Zheng
6 et al., 2015; Zheng and Rosenfeld, 2015). **From Figure 7, it is clearly observed that an overestimation**
7 **(difference observed between DL and CM CBH~ 0.5 km) of CBH is done by the DL in comparison to CM.**
8 **This could be due to different technical specification and retrieval techniques of both instruments. Similarly,**
9 **we have also observed the difference between LCL and derived CBH because of their retrieval techniques.**

10 In Figure 8, we have plotted the temporal variation of CBH with cloud base vertical velocity for all cases.
11 CBH observed with both the instruments are showing similar temporal variation throughout the observational time
12 period (10.5-15.5 LT). From figure 8(a-f), it is clearly evident that the updrafts are dominant due to the diurnal
13 evolution of convective ABL during daytime over the site. **The observed diurnal pattern of the vertical velocity**
14 **with DL for all the cases are showing the dominance of updrafts over the site.** In some cases like 12 October
15 2011, 21 November 2011 and 08 February 2012, the vertical velocity follows the similar pattern. We have also
16 plotted the temporal variation of cloud base vertical velocity with cloud base vertical velocity updraft fraction (m)
17 for all cases in Figure 9 (a-f). From this figure, it is clearly seen that both the parameter are well correlated. We have
18 also compared the CBH calculated by the DL and CM with the MODIS derived CBH for all cloud passes over the
19 observational site. For instance, Figure 10 shows the MODIS Terra derived CBH and the daily mean (05-10 UT)
20 CBH measured by the DL and CM. We have taken the mean of latitude/longitude ± 1 degree by centering the
21 latitude/longitude of the observational site. The observed CBH from MODIS is well within the estimated standard
22 deviation from ground based CBH. It shows reasonably good agreement with the estimation of CBH from the
23 ground based and DL and CM CBH in all the cases except in two cases (21 November 2011 and 14 March 2012)
24 where the differences are slightly higher and need to be investigated for the possible inconsistencies. **In Figure 10,**
25 **we have observed an overestimation of the MODIS CBH with respect to error bars of the observed CBH**
26 **from DL and CM. This overestimation of CBH by the MODIS could be due to the overpass and large spatial**
27 **grid.**

28 Further, we have used the DL and CM CBH as well as cloud updraft and cloud base vertical velocity
29 observed by the DL for all six cases to see the correlation which is plotted in Figure 11. The correlation of CBH
30 between the DL and CM is shown in Figure 11a. It is noticed that the CBH estimated by the DL is well correlated
31 ($R^2=0.81$) with the CM measured CBH when we combine all the cases shown in Figure 11a. We have observed
32 differences between the CBH DL and CM ~ 500 m which represents an overestimation of CBH by DL in
33 comparison to CM. These differences could be due to different methodologies for the estimation of CBH with both
34 the instruments and to the complex topography itself. ABL also plays an important role in the formation of clouds
35 and all the cases are during convective boundary layer conditions and this may be one of the reason behind the
36 overestimation with the DL in some cases. In addition, Figure 11b illustrates the relation between cloud base vertical
37 velocity and cloud updraft fraction observed by DL for all cloud passes over the observational site. As indicated in

1 Figure **11b**, a strong **correlation ($R^2=0.71$)** is also noted between these two parameters. Further, it is noticed that
2 when the cloud updraft fraction is less than 40%, the cloud base vertical velocity tends to be negative. However,
3 positive vertical velocities are noted when the cloud updraft fraction is more than 50%. Kollias et al. (2001) showed
4 that the cloud base vertical velocity is consistent with the updraft speed. We have also observed similar behavior
5 between the cloud base vertical velocity and updraft fraction although our observations are from a high altitude
6 location. Jeong and Li (2010) estimated the CBH by using micropulse Lidar for few case studies by applying the
7 threshold condition of aerosol particle diameter less than 1 μm and relative humidity 40 % over the southern great
8 plain site. They have observed the cumulus cloud on all cases and found the CBH varying in between 1-4 km, above
9 mean sea level (amsl). A detailed comparison of CBH estimated over various parts of the world by using different
10 ground based instruments and satellite datasets is shown in Table-2. Despite different site morphologies, our CBH
11 values observed with both DL and CM (Table-2) are in agreement with past studies across the globe. Bühl et al.,
12 (2015) observed the cloud and vertical velocity by using different ground based instruments e.g. DL, cloud radar and
13 wind profiler over meteorological observatory, Lindenberg, Germany.

14 The cloud observations **with DL & CM during all case examples show that CBH varies between ~ 2-3 km,**
15 **above mean sea level (amsl) over the site.** The presence of **higher magnitude (high positive vertical velocity)**
16 updrafts in the cloud layers was also observed. The observed vertical velocity in the cloud layer varied between \pm
17 1.5 ms^{-1} . Similar characteristics were observed at Manora Peak, Nainital. We have observed that cloud base vertical
18 velocity varies between $\pm 2 \text{ ms}^{-1}$ except for 20 January 2012 during which higher vertical velocities of $0-4 \text{ ms}^{-1}$ were
19 obtained. The observed CBH also varies between 2.3-2.7 km amsl in both instruments over Manora Peak, Nainital.
20 Hirsch et al. (2011) retrieved the CBH by CM, and observed the shallow cumulus cloud during daytime and CBH at
21 $1.6\pm 0.3 \text{ km}$, amsl. Also, Meerkötter and Bugliaro, (2009) estimated the CBH by using MSG/SEVIRI, NOAA
22 satellite data and CM data for convective cloud cases over the seven test stations near Germany and neighboring
23 countries. By using geostationary satellite and ground based CMs, they have observed that CBH varies between ~
24 2-3 km and also showed a significant correlation. Thus, our results are in good agreement with the temporal
25 variation of CBHs observed by DL compared with CM in previous studies. **The cooling and warming of the**
26 **atmosphere is governed by the presence of clouds at different altitudes in the atmosphere (Kiehl and**
27 **Trenberth, 1997).** **CBH of low level clouds coupled with shallow convection is playing an essential role in the**
28 **parameterization of weather and climate models (Chandra et al., 2015).** **Also the uncertainty observed in**
29 **climate models is due to low-level clouds (Bony and Dufresne, 2005) especially when model grid spacing is**
30 **much larger than the size of low level. Therefore, the continuous estimation of CBH will be a useful input for**
31 **the models. Further, the cloud radiative cooling, relative humidity in the ABL and cloud cover have direct**
32 **association with the low altitude clouds (Brient and Bony, 2012).** **Therefore, the accurate and systematic**
33 **measurements of low level cloud base become important for the improvement of the models. Hence, in this**
34 **report we investigated the potential of the DL in measuring the CBH over the site in comparison to CM.**
35 **From the current study, it is also clearly seen that we can use DL for CBH study over the site. It also**
36 **demonstrates that the precise observations of the CBH over the complex topography are very useful for**
37 **model validation.**

1
2
3
4
5
6
7
8
9
10
11
12
13
14
15
16
17
18
19
20
21
22
23
24
25
26
27
28
29
30
31
32
33
34
35

5. Summary and Conclusions

In this study, we have presented comparison of the CBH estimated by using the DL with CM and MODIS derived CBH over a high altitude site in the **foothills of the Himalayan mountain range** region. TSI shows the presence of cloud over the site for the cases evaluated in the current study and also opaque clouds are more frequently observed than thin clouds over the site during the observational period. The height-time variation of SNR of DL and backscatter by the CM depict a similar pattern for the cases evaluated with opaque (thin) clouds dominating during morning (afternoon) hours in most of the cases. Strong correlation ($R^2=0.81$) between DL and CM CBH is observed suggesting that DL can also be used as a potential instrument for measuring CBH apart from standard instrument CM. Similarly, we have observed the good correlation ($R^2=0.71$) between cloud base vertical velocity and cloud updraft fraction. We have observed a similar temporal variation between CBH (estimated from DL and CM) and LCL height (Surface MET and RS) during all the cases. The CBH height and LCL height derived from surface MET and RS are also comparable. The estimated CBH with the MODIS data is also in close agreement with the ground based instruments in most of the observed cases.

Further, our results also show close agreement with the CBH derived by DL, CM and MODIS derived satellite data sets in all cases. **We have also noticed an overestimation (~ 500 m) of CBH by DL in comparison to CM which is due to different technical specifications of the instruments and different retrieval methodologies of CBH. Similarly, a difference is observed between the MODIS derived CBH and DL, CM derived CBH mainly due to the large spatial grid and overpass time of the MODIS over the observational site. By considering the importance of the current study, CBH estimations by DL along with the cloud updraft velocities will be utilized in our future studies as potential inputs for numerical weather prediction models over the foothills of the Himalayan mountain range region.**

Acknowledgments

This work has been carried out as a part of GVAX campaign under joint collaboration among Atmospheric Radiation Measurement (ARM), Department of Energy (US), Indian Institute of Science (IISc) and Indian Space Research Organization (ISRO), India. We thank Director, ARIES for providing the necessary support. We also thank MODIS team for providing the valuable datasets used in the present study. The authors wish also to thank the Associate Editor, for his judicious comments which helped improve the quality of the paper. **The authors thank to Victor Morris for his detailed discussion regarding the Total Sky Imager (TSI) and his inputs to improve the quality of work.**

1
2
3
4
5
6
7
8
9
10
11
12
13
14
15
16
17
18
19
20
21
22
23
24
25
26
27
28
29
30
31
32
33
34
35
36
37

References

Asnani, G. C., Climatology of the tropics, in Tropical Meteorology, vol. 1, pp. 100–204, 2005.

Berg, L. K., and Kassianov, E. I.: Temporal variability of fair-weather cumulus statistics at the ACRF SGP site, *J. Climate*, 21, 3344-3358, 2008.

Bhat, G. S. and Kumar, S.: Vertical structure of cumulonimbus towers and intense convective clouds over the South Asian region during the summer monsoon season, *J. Geophys. Res.-Atmos.*, 120, 1710-1722, 2015.

Bollasina, M A, Y Ming, and V Ramaswamy: Anthropogenic aerosols and the weakening of the South Asian summer monsoon, *Science* 334(6055): 502–505, 2011.

Bony, S., and Dufresne, J. L.: Marine boundary layer clouds at the heart of tropical cloud feedback uncertainties in climate models, *Geophys. Res. Lett.*, 32, L20806, 2005.

Brient, F., and Bony, S.: Interpretation of the positive low cloud feedback predicted by a climate model under global warming. *Clim. Dyn.*, 40: 2415, 2012.

Brown, A. R., et al.: Large-eddy simulation of the diurnal cycle of shallow cumulus convection over land, *Q. J. R. Meteorol. Soc.*, 128, 1075-1093, 2002.

Bühl, J., Leinweber, R., Görtsdorf, U., Radenz, M., Ansmann, A., and Lehmann, V.: Combined vertical-velocity observations with Doppler Lidar, cloud radar and wind profiler, *Atmos. Meas. Tech.*, 8, 3527-3536, 2015.

Chandra, A. S., C. Zhang, S. A. Klein, and H.-Y. Ma: Low-cloud characteristics over the tropical western Pacific from ARM observations and CAM5 simulations, *J. Geophys. Res. Atmos.*, 120, 2015.

Considine, G., Curry, Judith A., and Wielicki, Bruce: Modeling cloud fraction and horizontal variability in marine boundary layer cloud, *J. Geophys. Res.*, 102, 13517-13525, 1997.

Crum, T. D., and Stull, R. B.: Field measurements of the amount of surface layer air versus height in the entrainment zone, *J. Atmos. Sci.*, 44(19), 2743–2753, 1987.

Craven, J. P., Jewell, R. E., and Brooks, H. E.: Comparison between observed convective cloud-base heights and lifting condensation level for two different lifted air parcels, *Weather Forecast.*, 17, 885–890, 2002.

Dumka et al.: Seasonal in homogeneity in cloud precursors over Gangetic Himalayan region during GVAX campaign, *Atmos. Res.*, 155,158-175, 2014.

Emeis, S, K Schäfer, and Münkel, C.: Observation of the structure of the urban boundary layer with different ceilometers and validation by RASS data. *Meteorologische Zeitschrift* 18: 49-154, 2009.

Flynn, C.: Vaisala Ceilometer (Model CT25K) Handbook, ARM TR-020, 2004.

Forsythe, J. M., Vonder Haar, T. H., and Reinke, D. L.: Cloud-Base Height Estimates Using a Combination of Meteorological Satellite Imagery and Surface Reports, *J. Appl. Meteorol.*, 39, 2336–2347, 2000.

Ghate, Virendra P., Mark A. Miller, and Lynne Di Pretore: Vertical velocity structure of marine boundary layer trade wind cumulus clouds, *J. Geophys. Res.*, 116, D16206, 2011.

Goff, J. A. and Gratch, S.: Low-pressure properties of water from -160 to 212 °F. *Trans. Amer. Soc. Heating Vent. Eng.*, 95-122, 52nd Annual Meeting, NewYork, 1946.

1 **Haeffelin, M., F. Angelini, Y. Morille, G. Martucci, S. Frey, G. P. Gobbi, S. Lolli, C. D. O’Dowd, L. Sauvage,**
2 **I. Xueref-Remy, B. Wastine, and D. G. Feist: Evaluation of Mixing-Height Retrievals from Automatic**
3 **Profiling Lidars and Ceilometers in View of Future Integrated Networks in Europe, *Boundary-Layer***
4 ***Meteorol*, 143:49-75, 2012.**

5 Hess, M., Koepke P. and Schult I.: Optical Properties of Aerosols and clouds: The Software Package OPAC., B.
6 *Am. Meteorol. Soc.*, 79, 5, 831-844, 1998.

7 Heymsfield, A.J.: Microphysical structures of stratiform and cirrus clouds, *Aerosol-Cloud-Climate Interactions*, P.
8 Hobbs, Ed., *International Geophysics Series*, Vol 54, Academic Press, 97-121, 1993.

9 Hirsh, E., E. Agassi and Koren, I.: A novel technique for extracting clouds base height using ground based imaging.
10 *Atmos. Meas. Tech.*, 4,117-130, 2011.

11 Holdridge, Donna J., Prell, Jenni A., Ritsche, Michael T. and Coulter, Rich : Balloon-Bourn sounding system
12 Handbook, DOE/SC-ARM-TR-029, 2011.

13 Huang, J.-P., P. Minnis, B. Lin, T. Wang, Y. Yi, Y. Hu, S. Sun-Mack, and Ayers, K.: Possible influences of Asian
14 dust aerosols on cloud properties and radiative forcing observed from MODIS and CERES, *Geophys. Res. Lett.*, 33,
15 L06824, doi: 10.1029/2005GL024724, 2006.

16 Hutchison, K.D.: The retrieval of cloud base heights from MODIS and three-dimensional cloud fields from NASA’s
17 EOS Aqua mission. *Int. J. Remote Sensing*, 23, 5249-5265, 2002.

18 **Illingworth, A. J., R. J. Hogan, E. J. O’Connor, D. Bouniol, J. Delanoë, J. Pelon, A. Protat, et al.: Cloudnet:**
19 **Continuous Evaluation of Cloud Profiles in Seven Operational Models Using Ground-Based Observations.**
20 ***Bull. Amer. Meteor. Soc.*, 88 (6): 883-898, 2007.**

21 Jeong, M. J., and Li, Z.: Separating real and apparent effects of cloud, humidity, and dynamics on aerosol optical
22 thickness near cloud edges, *J. Geophys. Res.*, 115, D00K32, 2010.

23 Jones, C. R., Bretherton, C. S., and Leon, D.: Coupled vs. decoupled boundary layers in VOCALS-REx, *Atmos.*
24 *Chem. Phys.*, 11, 7143–7153, doi: 10.5194/acp-11-7143-2011, 2011.

25 Kiehl, J. T. and Trenberth, K. E.: Earth’s Annual Global Mean Energy Budget, *B. Am. Meteorol. Soc.*, 78, 197-208,
26 1997.

27 **Kishcha, P., Starobinets, B. and Alpert, P.: Latitudinal variations of cloud and aerosol optical thickness**
28 **trends based on MODIS satellite data. *Geophys. Res. Lett.*, 34, L05810, 2007.**

29 Koehler, T. L., R. W. Johnson, and Shields, J. E.: Status of the whole sky imager database. *Proc. Cloud Impacts on*
30 *DOD Operations and Systems-1991 Conference*, El Segundo, CA, Department of Defense, 77–80, 1991.

31 Kollias, P., B. A. Albrecht, R. Lhermitte, and Savtchenko, A.: Radar observations of updrafts, downdrafts, and
32 turbulence in fair-weather cumuli. *J. Atmos. Sci.*, 58, 1750–1766, 2001.

33 Kotamarthi, V. R.: Ganges Valley Aerosol Experiment: Science and Operations Plan, DOE/SC-ARM-10-019, June
34 2010.

35 Kotamarthi, V. R.: Ganges Valley Aerosol Experiment (GVAX) Final Campaign Report. DOE/SC-ARM-14-011,
36 2013.

1 Kummerow, C., Barnes, W., Kozu, T., Shiue, J., and Simpson, J.: The Tropical Rainfall measuring Mission
2 (TRMM) Sensor Package, *J. Atmos. Ocean. Tech.*, 15, 809–817, 1998.

3 Lau, K M, and K M Kim: Observational relationships between aerosol and Asian monsoon rainfall, and circulation,
4 *Geophys. Res. Lett.*, 33: L21810, 2006.

5 **Lawrence, M.: The relationship between relative humidity and the dew point temperature in moist air: A**
6 **simple conversion and applications. *Bull. Amer. Meteor. Soc.*, 86, 225-233, 2005.**

7 **Lenschow D.H., Wulfmeyer, V., Senff, C.: Measuring Second- through Fourth-Order Moments in Noisy**
8 **Data. *J. Atmos. Ocean. Tech.*, 17, 1330-1347, 2000.**

9 Long, C. N., D. W. Slater, and Tooman , T.: Total Sky Imager Model 880 Status and Testing Results. ARM
10 Technical Report ARM TR-006, U.S. Department of Energy, Washington, D.C, 2001.

11 Liou, K-N.: *Radiation and Cloud Processes in the Atmosphere* (Oxford: Oxford University Press), 1992.

12 Long C.N., Sabburg, J.M., Calbo, J. and Pages, D.: Retrieving cloud characteristics from Ground-based daytime
13 color all-sky image. *J. Atmos. Oceanic Technol.*, 23, 633-652, 2006.

14 **Manninen A. J., O'Connor, Ewan J., Vakkari, Ville, and Petäjä, Tuukka: A generalised background**
15 **correction algorithm for a Halo Doppler lidar and its application to data from Finland, *Atmos. Meas. Tech.*,**
16 **9, 817-827, 2016.**

17 **Martucci, G. et al.: Detection of Cloud-Base Height Using Jenoptik CHM15K and Vaisala CL31 Ceilometer,**
18 ***J. Atmos. Ocean. Tehcnol.* 27, 305-318, 2010.**

19 Meerkötter, R. and Bugliaro, L.: Diurnal evolution of cloud base heights in convective cloud fields from
20 MSG/SEVIRI data, *Atmos. Chem. Phys.*, 9, 1767-1778, 2009.

21 Morris Victor: Total Sky Imager Handbook, DOE/SC-ARM-TR-017, 2005.

22 Morris V.R.: Vaisala Ceilometer (VCEIL) Handbook, DOE/SC-ARM-TR-020, 2012.

23 **Münkel, C., Eresmaa, N., Räsänen, J., and Karppinen, A.: Retrieval of mixing height and dust concentration**
24 **with lidar ceilometer, *Bound.-Lay. Meteorol.*, 124, 117–128, doi:10.1007/s10546-006-9103-3, 2007.**

25 **Münkel, C., Schäfer, K., and Emeis, S.: Adding confidence levels and error bars to mixing layer heights**
26 **detected by ceilometer, *Proc. SPIE* 8177, 817708–1 – 817708–9, 2011.**

27 Newsom R. K.: Doppler Lidar (DL) Handbook, DOE/SC-ARM-TR-101, 2012.

28 Newsom, R.K., Sivaraman, C., Shippert, T.R. and Riihimaki, L.D.: Doppler Lidar vertical velocity statistics value-
29 added product, DOE/SC-ARM-TR-149, 2015.

30 **O'Connor et al., 2010, "A Method for Estimating the Turbulent Kinetic Energy Dissipation Rate from a**
31 **Vertically Pointing Doppler Lidar, and Independent Evaluation from Balloon-Borne In Situ Measurements",**
32 ***J. Atmos. Ocean. Tech.*, 27.**

33

34 Pearson, G.N., Davies, F., Collier, C.: An analysis of the performance of the UFAM pulsed Doppler Lidar for
35 observing the boundary layer. *J.Atmos.Oceanic Technol.*, 26, 240-250, 2009.

1 Pfister, G., R. L. McKenzie, J. B. Liley, A. Thomas, B. W. Forgan, and Long, C. N.: Cloud coverage based on all-
2 sky imaging and its impact on surface solar irradiance. *J. Appl. Meteor.*, 42, 1421-1434, 2003.

3 **Platnick, Steven, Michael D. King, Kerry G. Meyer, Gala Wind, Nandana Amarasinghe, Benjamin**
4 **Marchant, G. Thomas Arnold, Zhibo Zhang, Paul A. Hubanks, Bill Ridgway, Jérôme Riedi.: MODIS Cloud**
5 **Optical Properties: User Guide for the Collection 6 Level-2 MOD06/MYD06 Product and Associated Level-3**
6 **Datasets. Version-1,http://modis-atmos.gsfc.nasa.gov/_docs/C6MOD06OPUserGuide.pdf, 2015.**

7 Ramanathan, V, C Chung, D Kim, T Bettge, L Buja, JT Kielh, WM Washington, Q Fu, DR Sikka, and M Wild.
8 2005: Atmospheric brown clouds: Impacts on South Asian climate and hydrological cycle. *Proceedings of the*
9 *National Academy of Sciences* 102: 5326-5333, 2005.

10 Randall, D. A., J. A. Abeles and Corseti, T. G.: Seasonal simulations of the planetary boundary layer and boundary
11 layer stratocumulus with a general circulation model. *J. Atmos. Sci.* 42, 641-676, 1985.

12 Ritsche, Michael T. and Prell, Jenni (2011), *ARM Surface Meteorology Systems Handbook*,
13 DOE/SC-ARM-TR-086, 2011.

14 Sagar, R., Dumka, U. C., Naja, M., Singh, N., Phanikumar, D. V.: ARIES, Nainital: a strategically important
15 location for climate change studies in the central Gangetic Himalayan region. *Current Science*, Vol. 109, No. 4, 25
16 August 2015.

17 Sarangi, T., Naja, M., Ojha, N., Kumar, R., Lal, S., Venkataramani, S., Kumar, A., Sagar, R. and Chandola, H. C.:
18 First simultaneous measurements of ozone, CO, and NO_y at a high-altitude regional representative site in the
19 central Himalayas, *J. Geophys. Res. Atmos.*, 119, 1592–1611, 2014.

20 **Schween, J. H., Hirsikko, A., Löhnert, U., and Crewell, S.: Mixing-layer height retrieval with ceilometer and**
21 **Doppler lidar: from case studies to long-term assessment, *Atmos. Meas. Tech.*, 7, 3685-3704, doi:**
22 **10.5194/amt-7-3685-2014, 2014.**

23 Sharma, S., Vaishnav, R., Shukla, M. V., Kumar, P., Kumar, P., Thapliyal, P. K., Lal, S., and Acharya, Y. B.:
24 Evaluation of cloud base height measurements from Ceilometer CL31 and MODIS satellite over Ahmedabad,
25 India, *Atmos. Meas. Tech.*, 9, 711-719, doi:10.5194/amt-9-711-2016, 2016.

26 Shukla et al.: Estimation of the mixing layer height over a high altitude site in Central Himalayan region by
27 using Doppler Lidar, *J. Atmos. Solar-Terrestrial Phys.*, 109, 48-53, 2014.

28 **Singh, Narendra, Solanki, Raman, Ojha, N., Naja, M., Dumka, U. C., Phanikumar, D. V. Sagar, Ram,**
29 **Satheesh, S. K., Moorthy, K. Krishna, Kotamarthi, V. R. and Dhaka, S. K.: Variations in the cloud-base**
30 **height over the central Himalayas during GVAX: association with the monsoon rainfall. *Current Science*,**
31 **111, 109-116, 2016.**

32 Stephens, G. L., Vane, D. G., Boain, R. J., Mace, G. G., Sassen, K., Wang, Z., Illingworth, A. J., O'Connor, E. J.,
33 Rossow, W. G., Durden, S. L., Miller, S. D., Austin, R. T., Benedetti, A., and Mitrescu, C.: The cloudsat mission
34 and the A-train, *B. Am. Meteorol. Soc.*, 83, 1771–1790, 2002.

35 Stull, R. B.: A fair-weather cumulus cloud classification scheme for mixed layer studies, *J. Clim. Appl. Meteorol.*
36 24, 49-56, 1985.

1 **Stull, R. B., and Eloranta, E.: A case study of the accuracy of routine, fair-weather cloud-base reports, Natl.**
2 **Weather Dig., 10(1), 19-24, 1985.**

3 Tonttila, J. et al.: Cloud base vertical velocity statistics: a comparison between an atmospheric mesoscale model and
4 remote sensing observation. *Atmos. Chem. Phys.*, 11, 9207-9218, 2011.

5 Väisälä Oyj: Ceilometer CT25K: User's guide, Väisälä Oyj, Vantaa, 2002.

6 **Van Tricht, K. et al.: An improved algorithm for polar cloud-base detection by ceilometers over the ice**
7 **sheets, *Atmos. Meas. Tech.*, 7, 1153-1167, 2014.**

8 Varikoden, Hamza, R. Harikumar, R. Vishnu, V. Sasi Kumar, S. Sampath, S. Murali Das and G. Mohan Kumar:
9 Observational study of cloud base height and its frequency over a tropical station, Thiruvananthapuram, using a
10 ceilometer, *I. J. Rem. Sens.*, 32, 8505-8518, 2011.

11 **Wiegner, M., Madonna, F., Biniotoglou, I., Forkel, R., Gasteiger, J., Geiß, A., Pappalardo, G., Schäfer, K.,**
12 **and Thomas, W.: What is the benefit of ceilometers for aerosol remote sensing? An answer from EARLINET,**
13 ***Atmos. Meas. Tech.*, 7, 1979-1997, doi: 10.5194/amt-7-1979-2014, 2014.**

14 Weisz, E., Li, J., Menzel, W. P., Heidinger, A. K., Kahn, B. H., and Liu, C.-Y.: Comparison of AIRS, MODIS,
15 CloudSat and CALIPSO cloud top height retrievals, *Geophys. Res. Lett.*, 34, L17811, 2007.

16 Winker, D. M., Pelon, J. R., and McCormick, M. P.: The CALIPSO mission: space borne lidar for observations of
17 aerosols and clouds, *Proc. SPIE*, 4893, 1-11, 2003.

18 Zheng, Y., D. Rosenfeld, and Li, Z.: Satellite inference of thermals and cloud-base updraft speeds based on retrieved
19 surface and cloud base temperatures, *J. Atmos. Sci.*, 72(6), 2411-2428, 2015.

20 Zheng, Y., and Rosenfeld, D.: Linear relation between convective cloud base height and updrafts and application to
21 satellite retrievals, *Geophys. Res. Lett.*, 42, 6485–6491, doi: 10.1002/2015GL064809, 2015.

22 **Zhang, Y., and Klein, S. A.: Factors controlling the vertical extent of fair-weather shallow cumulus clouds**
23 **over land: Investigation of diurnal-cycle observations collected at the ARM Southern Great Plains site, *J.***
24 ***Atmos. Sci.*, 70(4), 1297-1315, 2013.**

25
26
27
28
29
30
31
32
33
34
35
36
37

1 **Table-1 Technical specification of the Doppler Lidar operated over the Manora Peak during GVAX**

2

Manufacturer	Halo Photonics
Eye safety Class	1M
Wavelength	1.5 μm
Laser pulse energy	~100 μJ
Laser pulse width	200 ns
Pulse rate	15 kHz
Nyquist Velocity	19.4 ms^{-1}
Unambiguous range	10 km
Aperture	75 mm
Volume approximately	0.5 m^3
Power consumption	< 300 W
Mass approximately	85 Kg
Temporal resolution selectable from	0.1 to 30 seconds
Range gate size	18 to 60m
Velocity precision	< 20 cm s^{-1} for SNR > -17 dB
Minimum range	<100m, typically 75m
Scanning	Step-stare, full upper hemisphere
Enclosure	Weatherproof, temperature stabilized

3

4

5

6

7

8

9

10

1 **Table-2:** Comparison of cloud base heights with other locations around the world

Observational site (Latitude/longitude/elevation)	Instrument	Date	Cloud base height (km) (amsl)	References
Lindenberg, Germany.	Doppler Lidar, Cloud radar, wind profiler	30 July 2013	2.9 km	Bühl et al.,2015
Israel (31.89 ⁰ N , 34.81 ⁰ E, 60 m)	Ceilometer	22 April 2010	1.6±0.3 km	Hirsch et al., 2011
Southern Great Plain (36.6 ⁰ N , 97.5 ⁰ W)	Micro pulse Lidar	07, 13 and 22 May 2003	4.2, 1.6 and 1.3 km, respectively	Jeong and Li,2010
Seven test station near Germany and neighboring countries	MSG/SEVIRI NOAA Ceilometer	23,30 May and 30 July 2007	Between 2-3 km	Meerkötter and Bugliaro, 2009
Nainital, India (29.4 ⁰ N, 79.2 ⁰ E, 1958 m)	Ceilometer Doppler Lidar	12 Oct, 21 Nov, 11 Dec, 2011 20 Jan, 08 Feb, 14 Mar 2012	2.468 2.328 2.298 2.228 2.688 2.568 2.438 2.418 2.678 2.658 2.348 2.258	Current study

2 * Red color in table represents the CBH of Ceilometer

3

4

5

6

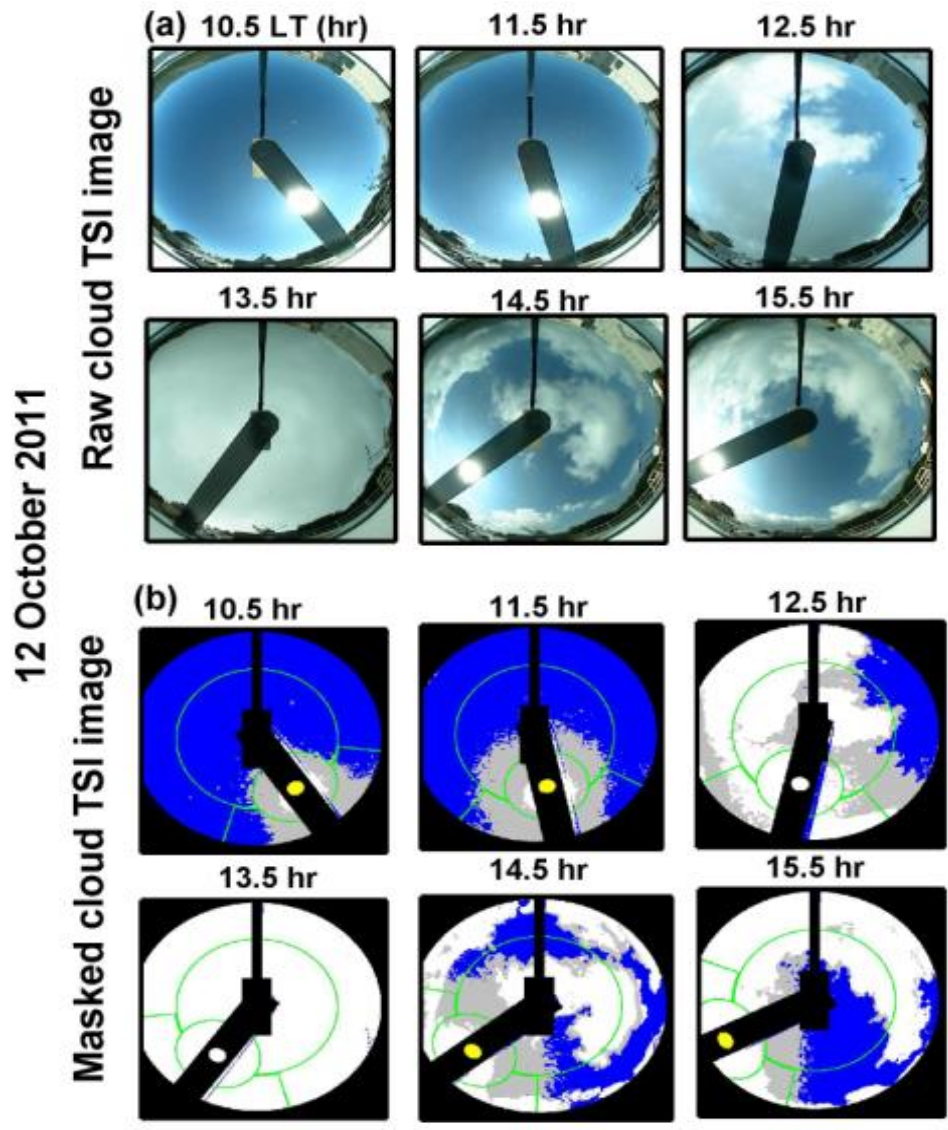
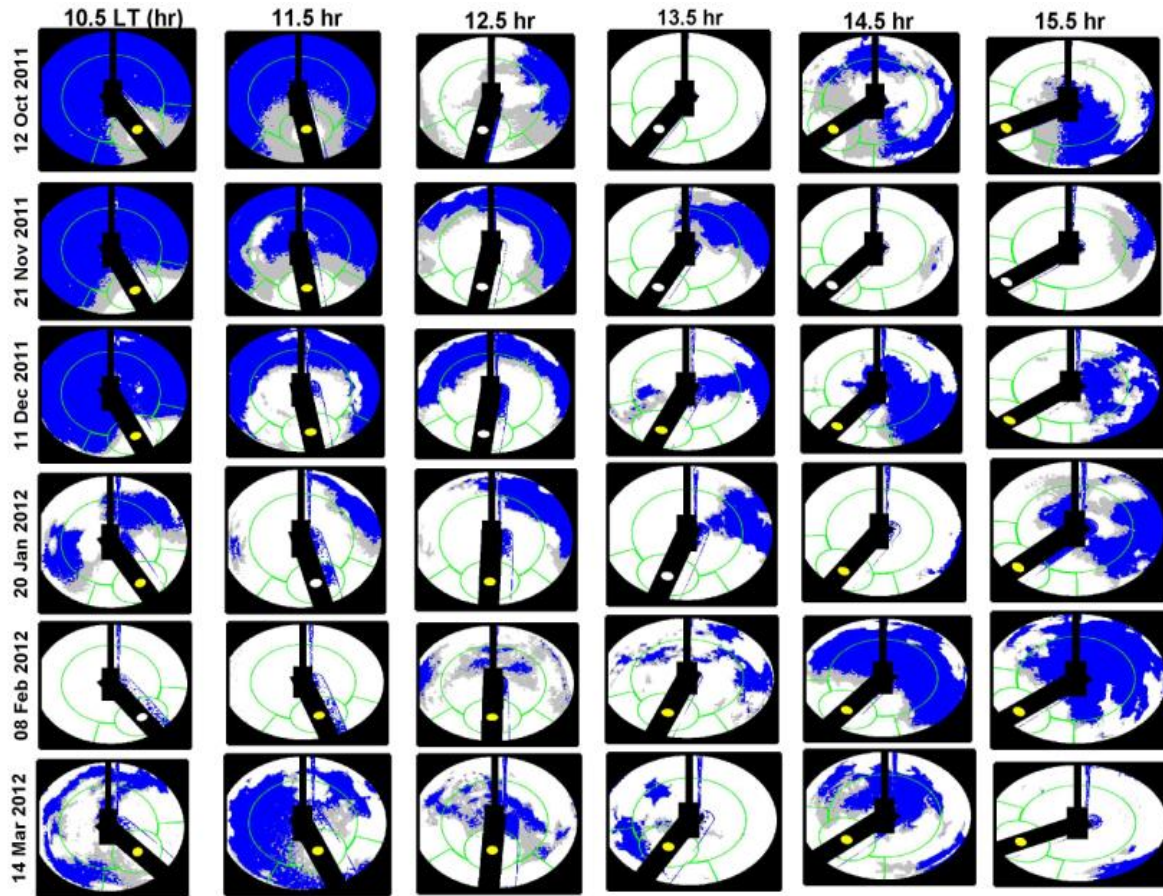


Figure 1: (a-b) Top panels show raw images of clouds during daytime observed by the TSI and bottom panels are the TSI cloud decision images. In the cloud decision images, blue, gray and white colors represent cloud-free sky, thin cloud and opaque clouds, respectively. Black color represents the masked pixels which are not used in the estimation of cloud property. The yellow dot on the sun-blocking strip mask represents the location of sun in the image.

1
2
3
4
5
6
7
8
9
10
11
12
13

1



2

3

4

5 **Figure 2:** Masked images of cloud during daytime (10.5-15.5 hr) taken by the TSI for (a) 12 October 2011, (b) 21
6 November 2011, (c) 11 December 2011, (d) 20 January 2012, (e) 08 February 2012, and (f) 14 March 2012. In the
7 cloud decision images, blue, gray and white colors represent cloud-free sky, thin cloud and opaque clouds,
8 respectively. Black color represents the masked pixels which are not used in the estimation of cloud property. The
9 yellow dot on the sun-blocking strip mask represents the location of sun in the image.

10

11

12

13

14

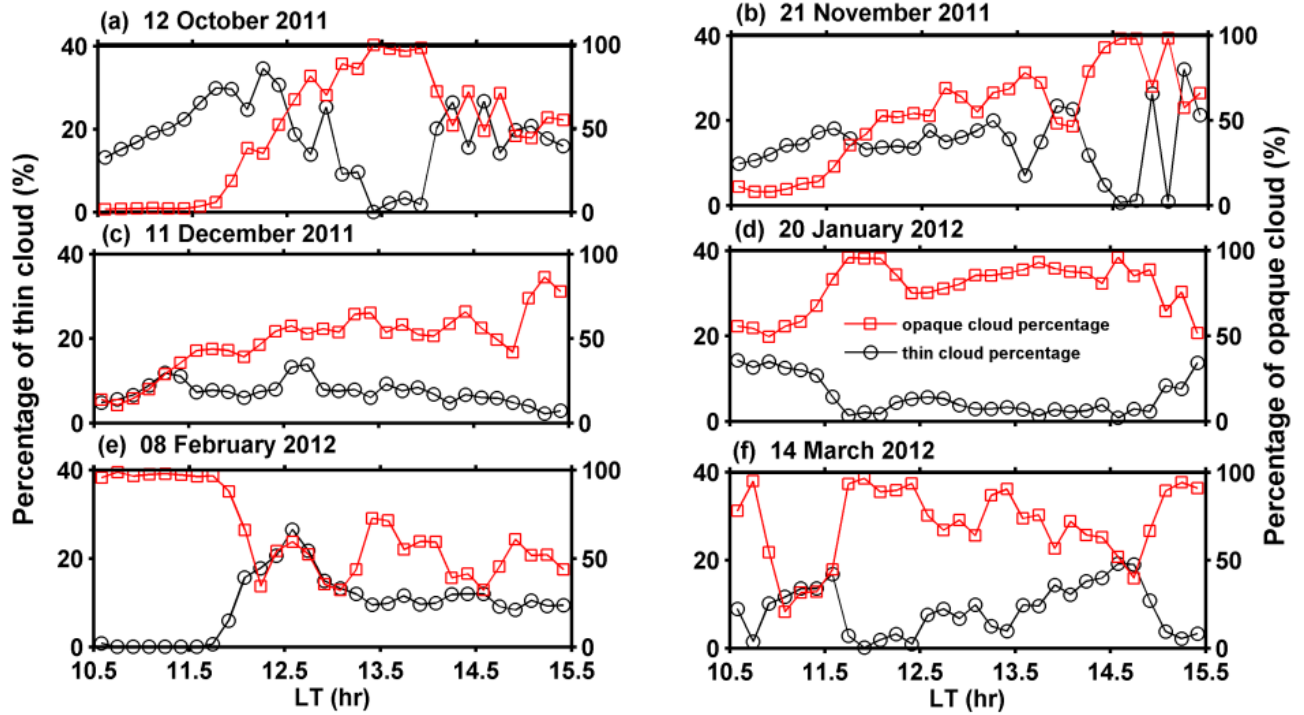
15

16

17

18

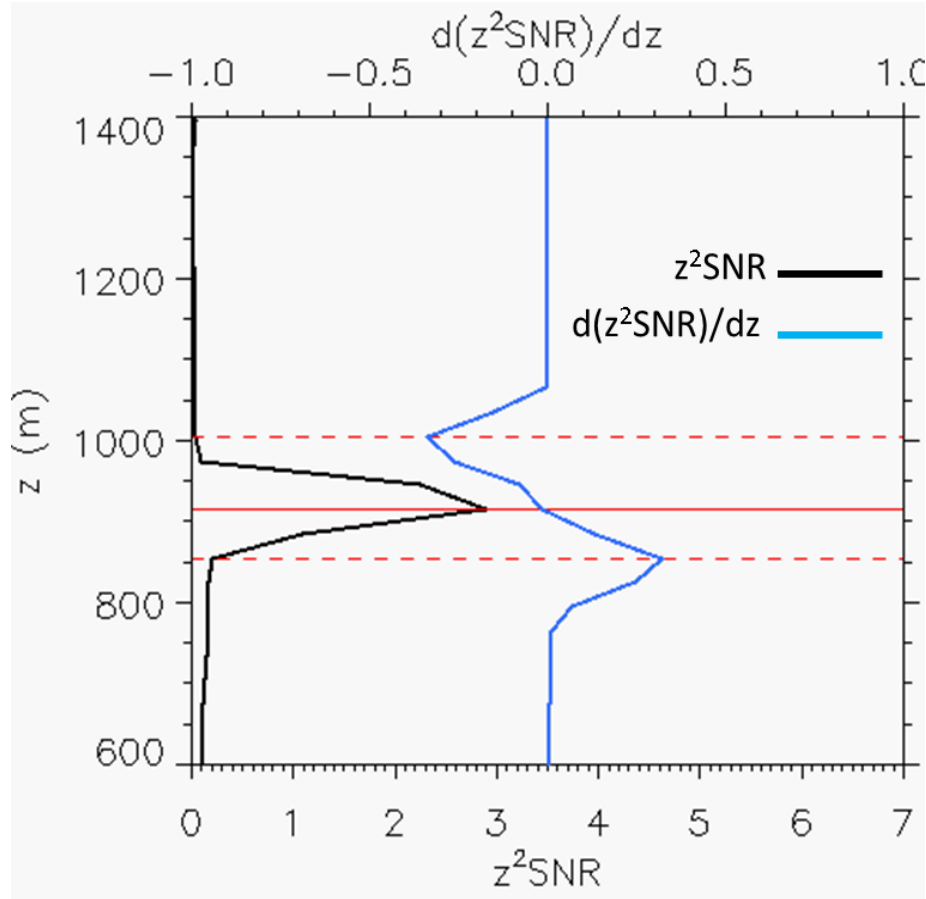
1
2
3
4



5
6
7
8
9
10
11
12
13
14
15
16
17
18
19
20
21

Figure 3: Temporal variation of (a) Percentage occurrence of thin clouds and (b) Opaque clouds observed by total sky imager over the site during (a) 12 October 2011, (b) 21 November 2011, (c) 11 December 2011, (d) 20 January 2012, (e) 08 February 2012, and (f) 14 March 2012.

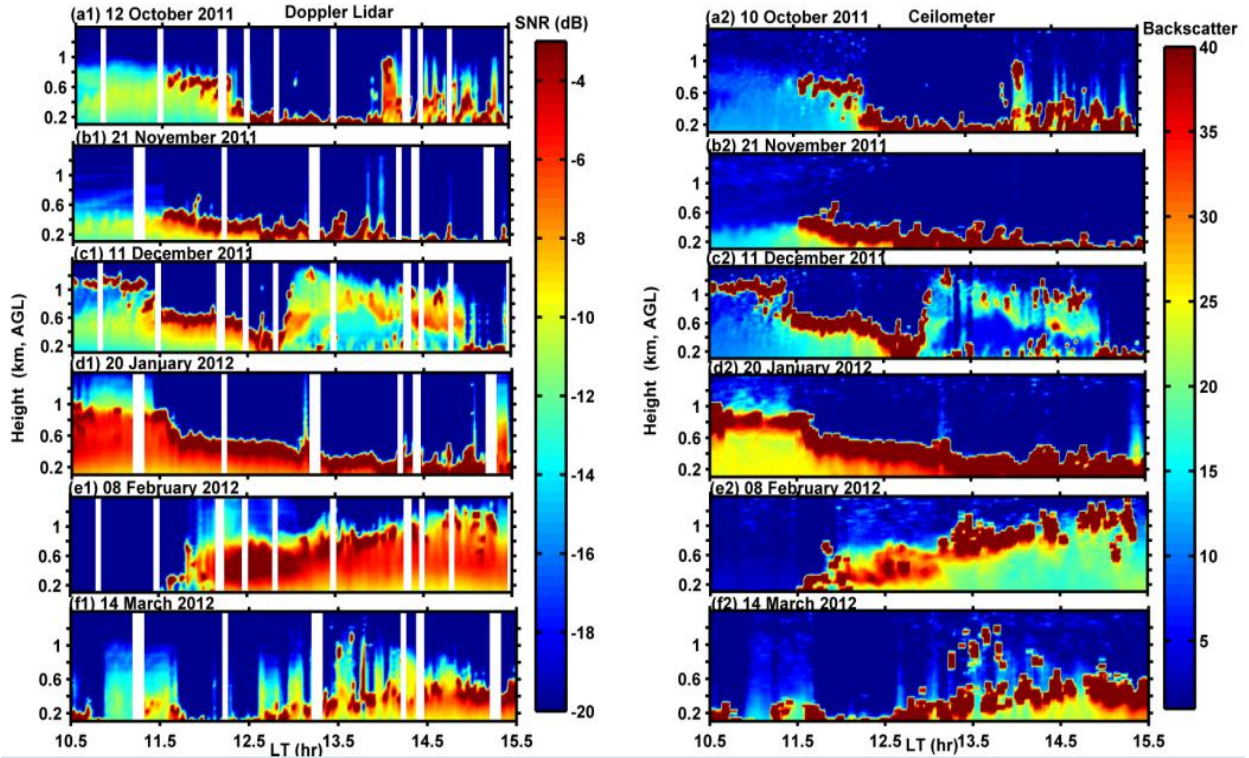
1
2
3
4



5
6
7
8
9
10
11
12
13
14
15
16
17
18

Figure 4. Example of the DL CBH detection method. The solid black curve is the range-corrected SNR, and the blue curve is the first derivative of the range-corrected SNR (based on the centered-difference approximation). The CBH (solid red line) is located by finding the maximum value of the range-corrected SNR between the heights corresponding to the minimum and maximum of the derivative (red dashed lines).

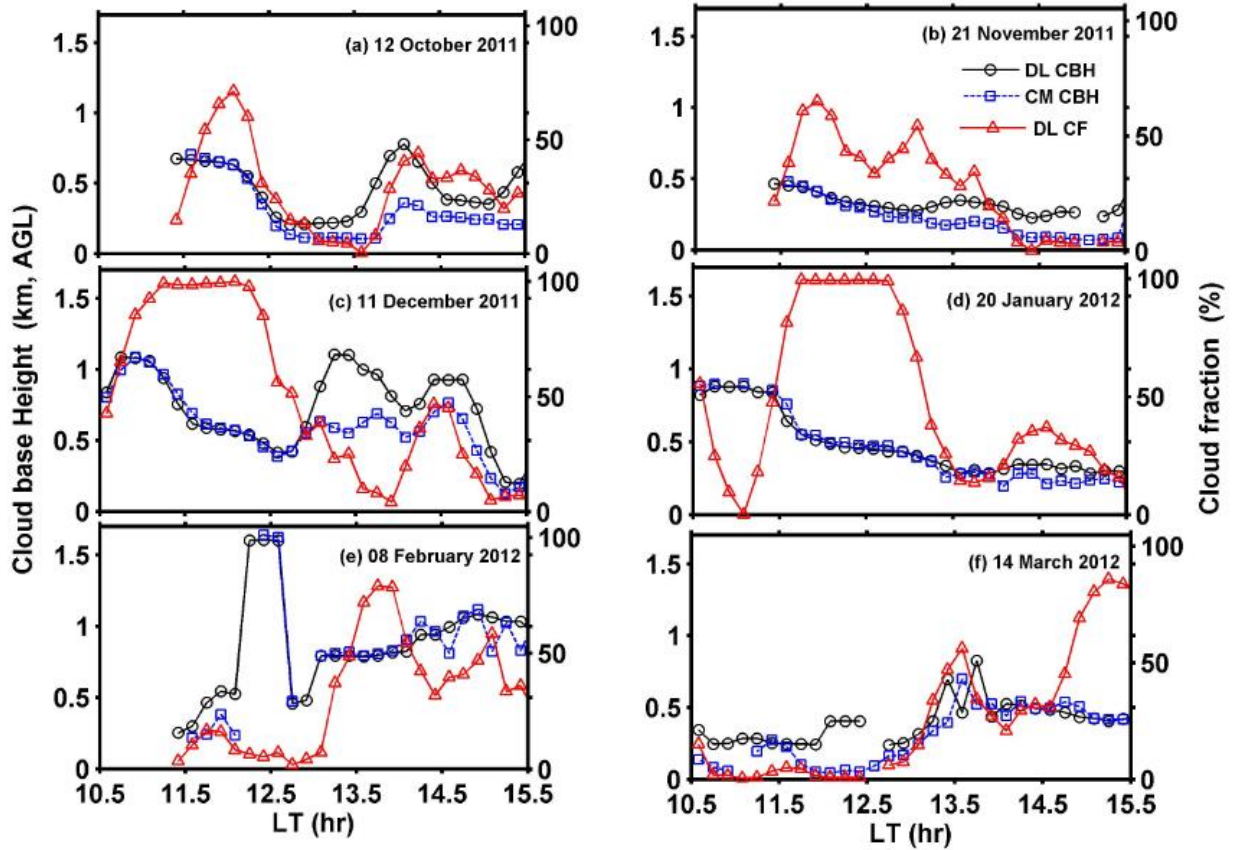
1
2
3
4
5
6



7
8
9
10
11
12
13
14
15
16
17
18
19
20
21

Figure 5: (a1-f1) Height-time variation of signal to noise ratio by Doppler Lidar and (a2-f2) Height-time variation of backscatter observed by the Ceilometer (colorbar represent the intensity of backscatter with different thickness of clouds observed by Ceilometer) during (a) 12 October 2011, (b) 21 November 2011, (c) 11 December 2011, (d) 20 January 2012, (e) 08 February 2012, and (f) 14 March 2012.

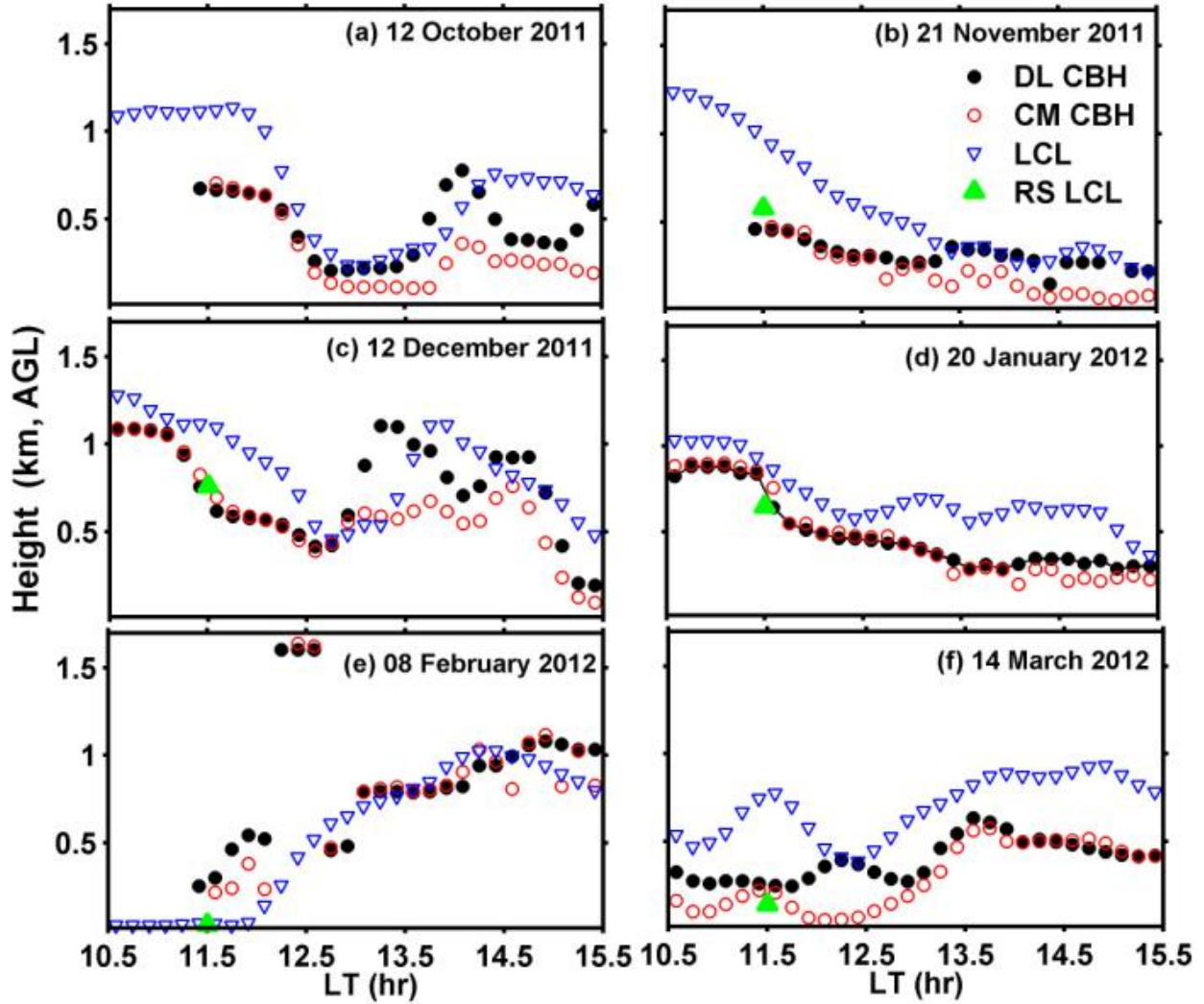
1
2
3
4
5
6
7



8
9
10
11
12
13
14
15
16
17
18
19

Figure 6: Temporal variation of cloud base height along with the cloud fraction observed by the Doppler Lidar observed during (a) 12 October 2011, (b) 21 November 2011, (c) 11 December 2011, (d) 20 January 2012, (e) 08 February 2012, and (f) 14 March 2012.

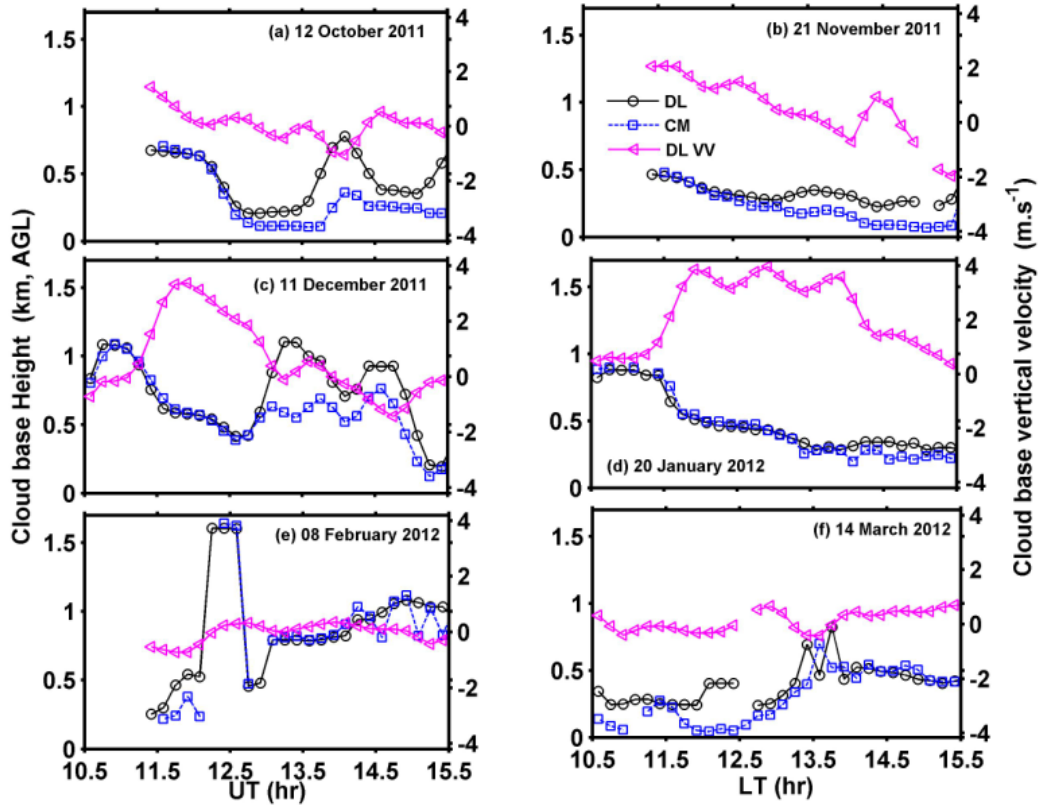
1
2
3
4



5
6
7
8
9
10
11
12
13
14

Figure 7: (a-f) Comparison of the cloud base height observed by Doppler Lidar and Ceilometer with lifting condensation level (LCL) estimated by the surface meteorological parameters and Radiosonde during (a) 12 October 2011, (b) 21 November 2011, (c) 11 December 2011, (d) 20 January 2012, (e) 08 February 2012, and (f) 14 March 2012.

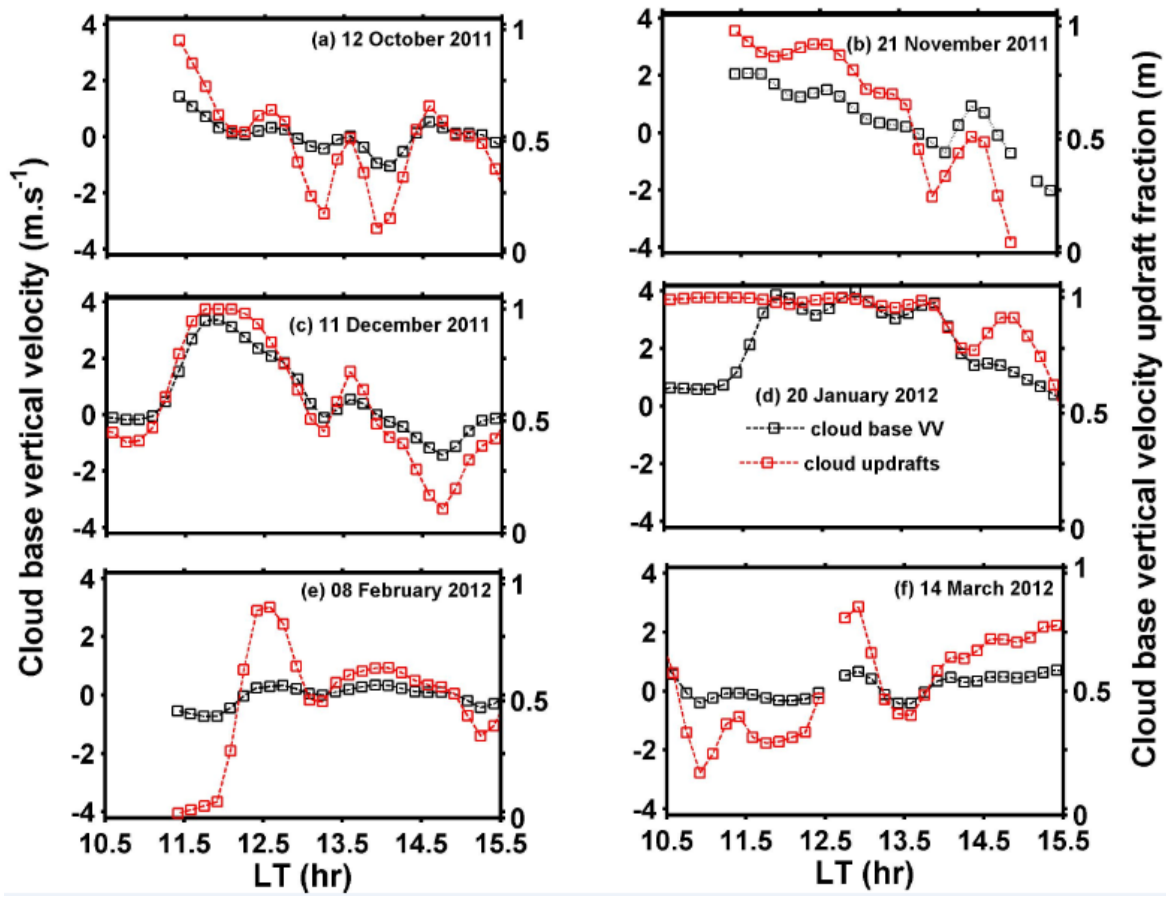
1
2
3
4
5
6
7
8



9
10
11
12
13
14
15
16
17
18
19
20

Figure 8: Temporal variation of CBH estimated by Doppler Lidar and Ceilometer with cloud base vertical velocity observed by the Doppler Lidar observed during (a) 12 October 2011, (b) 21 November 2011, (c) 11 December 2011, (d) 20 January 2012, (e) 08 February 2012, and (f) 14 March 2012.

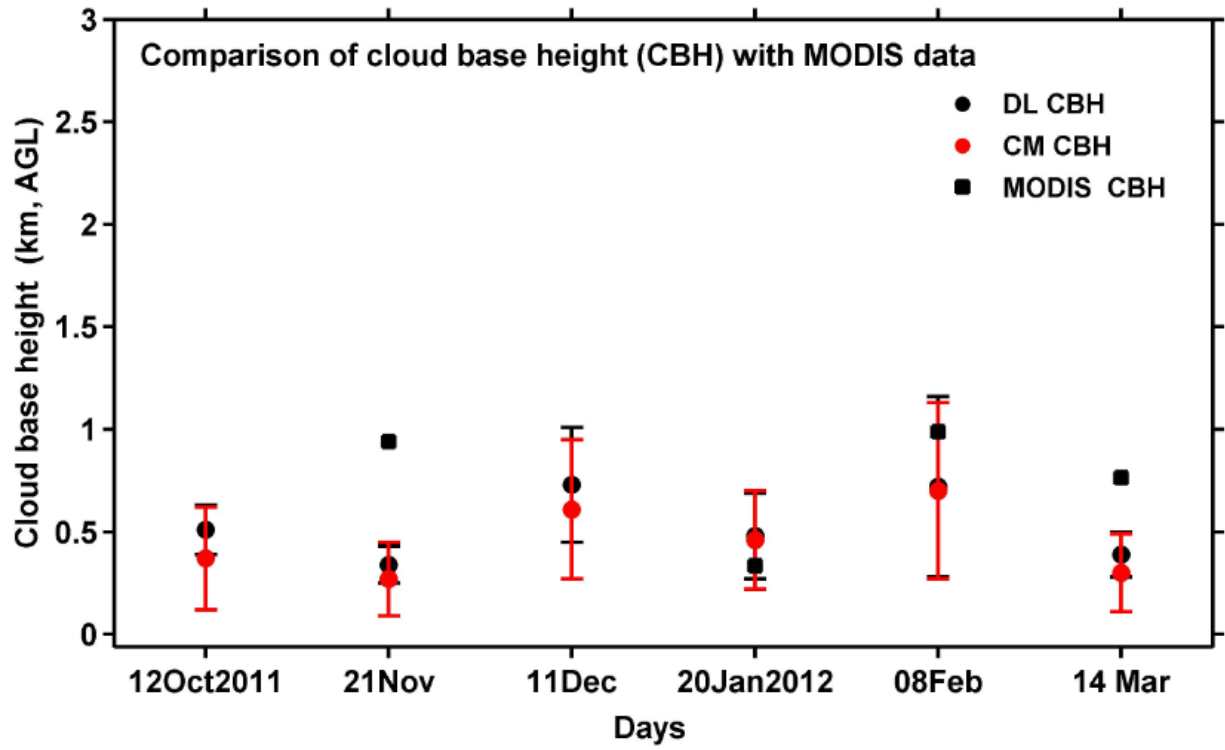
1
2
3
4
5
6
7
8
9



10
11
12
13
14
15
16
17
18

Figure 9: Temporal variation of cloud base vertical velocity along with cloud base vertical velocity updraft fraction observed during (a) 12 October 2011, (b) 21 November 2011, (c) 11 December 2011, (d) 20 January 2012, (e) 08 February 2012, and (f) 14 March 2012.

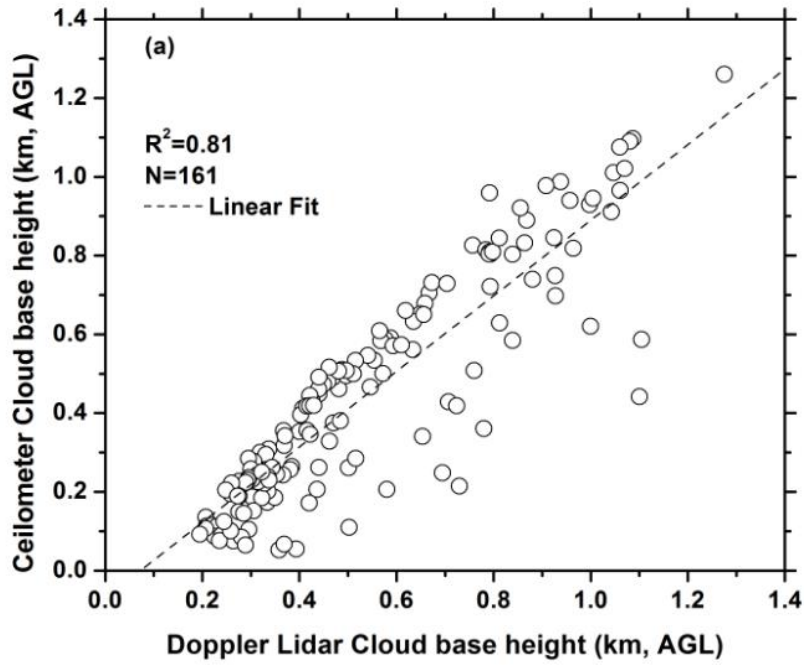
1
2
3
4
5
6
7
8
9



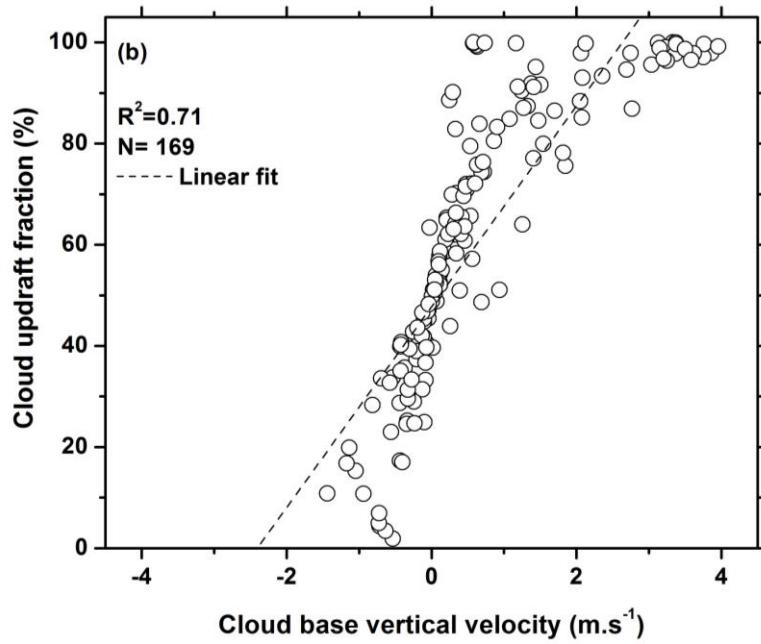
10
11
12
13
14
15
16
17
18
19
20
21

Figure 10: Comparison of cloud base height estimated by Doppler Lidar and Ceilometer during 10.5-15.5 LT and MODIS Terra centered at 10.30 LT during (a) 12 October 2011, (b) 21 November 2011, (c) 11 December 2011, (d) 20 January 2012, (e) 08 February 2012, and (f) 14 March 2012.

1
2



3



4
5
6
7
8
9

Figure 11: Co-relation between (a) the observed cloud base height from the Doppler Lidar and Ceilometer for all the above six cases during 10.5-15.5 LT (hr), and (b) Cloud base vertical velocity and Cloud updraft fraction measured by Doppler Lidar.